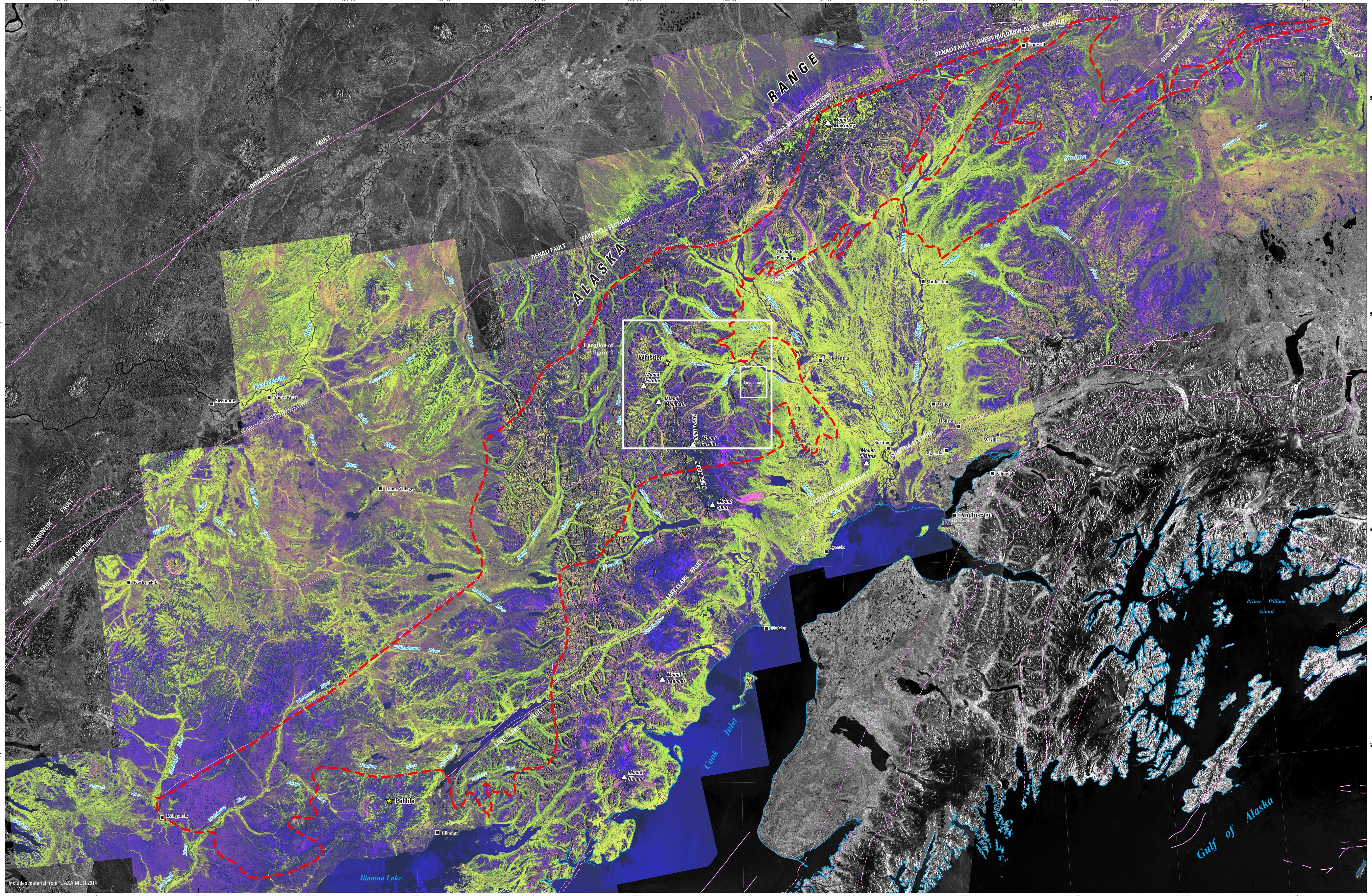

Base from 1:1,000,000 scale U.S. Geological Survey National Atlas (now National Map) digital data, accessed 2014 at *http://viewer.nationalmap.gov/viewer*

Base state boundary derived from U.S. Geological Survey digital data, 1:1,000,000 state boundaries of the United States
Cities and towns derived from U.S. Geological Survey digital data, 1:2,000,000 cities and towns of the United States

Projection: Universal Transverse Mercator, zone 5 north,
World Geodetic System 1984 datum (WGS 1984)

This product incorporates ALOS PALSAR Radar data which is ©Japan Aerospace Exploration Agency (JAXA) and the Japanese Ministry of Economy, Trade and Industry (METI), 2014.

APPROXIMATE MEAN DECLINATION AT CENTER OF MAP, 2014
DECLINATION RANGE 14.6 to 18.3 IN MAP AREA

SCALE 1:1 000 000

Digital cartography by C.J. Cole and M.R. Johnson, 2014.
Image base mosaic derived from ALOS PALSAR by C.J. Cole

PALSAR image patterns indicating land cover

- Barren land
- Forest
- Dwarf scrub and shrub/scrub
- Snow and ice
- Water

EXPLANATION

- **Faults**—Solid lines indicate where the fault is well constrained, dotted lines are inferred or concealed, and dashed where approximately located (modified from Plafker and others, 1994; Koehler and others, 2012)
- **Kahiltna terrane**—Late Jurassic to Early Cretaceous highly deformed basinal deep marine, partly volcaniclastic (granitic and dioritic), flyschoid graywacke and pelitic rocks (Silberling and others, 1994)
- **Shoreline**
- **City or town**
- **Named peak**
- **Pebble and Whistler deposit sites**—From Alaska Resource Data File (U.S. Geological Survey, 2008)

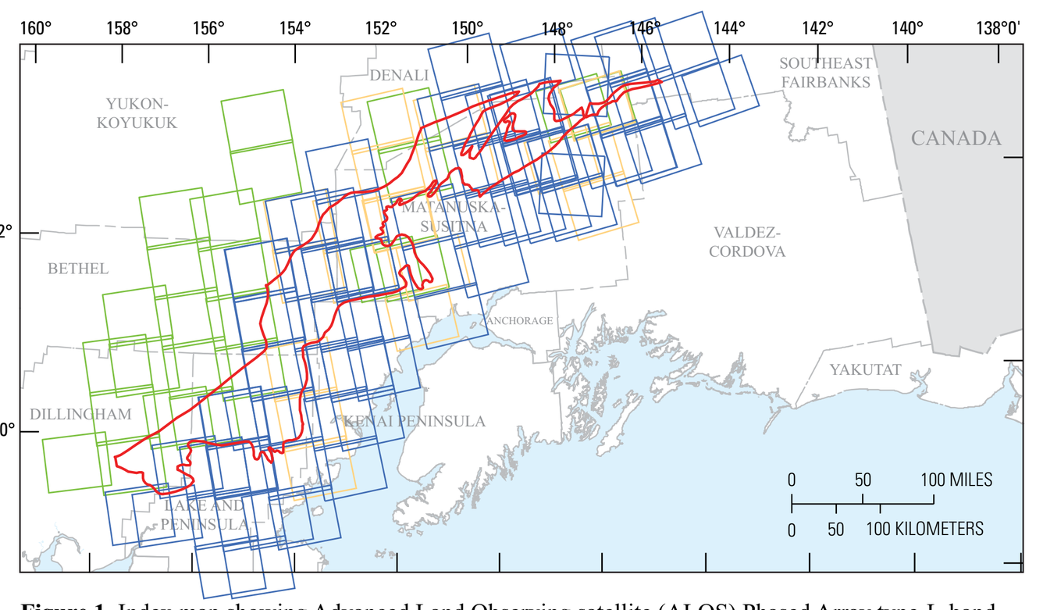

Figure 1. Index map showing Advanced Land Observing satellite (ALOS) Phased Array type-L-band Synthetic Aperture Radar (PALSAR) scenes used to create the radar mosaic for the Kahiltna terrane, Alaska.

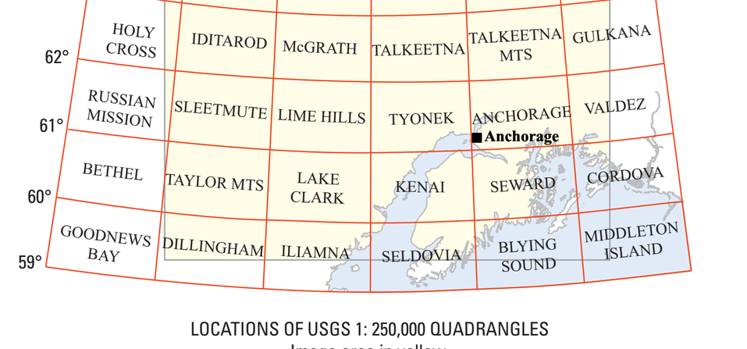

LOCATIONS OF USGS 1:250,000 QUADRANGLES
Image area in yellow

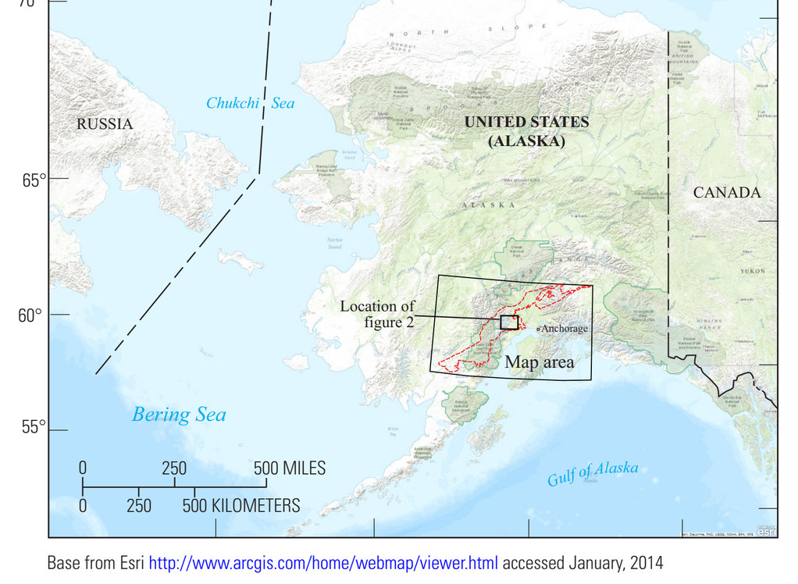

Location of map area. Red line indicates location of the Kahiltna terrane boundary (Silberling and others, 1994).

Advanced Land Observing Satellite (ALOS) Phased Array Type L-Band Synthetic Aperture Radar (PALSAR) Mosaic for the Kahiltna Terrane, Alaska, 2007–2010

By
Christopher J. Cole, Michaela R. Johnson, and Garth E. Graham
2015

Introduction

The U.S. Geological Survey (USGS) has initiated a multi-disciplinary study investigating the applicability of remote sensing technologies for geologic mapping and identification of prospective areas for base and precious metal deposits in remote parts of Alaska. The Kahiltna terrane in southwestern Alaska was selected for investigation because of its known mineral deposits and potential for additional mineral resources (Silberling and others, 1994; Graham and others, 2013).

An assortment of technologies is being investigated to aid in remote analysis of terrain, and includes imaging spectroscopy (hyperspectral remote sensing), high spatial resolution electro-optical imagery, and Synthetic Aperture Radar (SAR). However, there are significant challenges in applying imaging spectroscopy and electro-optical imagery technologies to this area because of the low solar angle for parts of the year, seasonal periods of darkness and snow cover, and the frequently cloudy weather that characterizes Alaska. Synthetic Aperture Radar (SAR) was selected because this technology does not rely on solar illumination and has all-weather capability.

The USGS has compiled a continuous, cloud-free 12.5-meter (m) resolution radar mosaic of SAR data of approximately 212,000 square kilometers (km^2) to examine the suitability of this technology for geologic mapping. This mosaic was created from Advanced Land Observing Satellite (ALOS) Phased Array type L-band Synthetic Aperture Radar (PALSAR) data collected from 2007 to 2010 spanning the Kahiltna terrane and the surrounding area (fig. 1). Interpretation of these data may help geologists understand past geologic processes and identify areas with potential for near-surface mineral resources for further ground-based geological and geochemical investigations.

Synthetic Aperture Radar (SAR)—Advanced Land Observing Satellite (ALOS) Phased Array Type L-Band Synthetic Aperture Radar (PALSAR)

Advanced Land Observing Satellite (ALOS) Phased Array Type L-Band Synthetic Aperture Radar (PALSAR), referred to as ALOS PALSAR, was launched in January 2006 and collected imagery until April of 2011 (Japan Space Systems, 2012). During its operation, the satellite-based sensor produced an image archive (https://www.asf.alaska.edu/sar-data/palsar/) which has been used for a wide range of scientific studies. PALSAR is a remote sensing technology measuring the microwave portion of the electromagnetic spectrum. As an "active" technology, solar illumination is not required during data collection. Therefore, collection of PALSAR data is not limited to daylight hours and is relatively insensitive to cloud cover and weather effects.

Like other polarimetric radar systems, ALOS PALSAR data can be used to derive Earth-surface information by exploiting multiple polarization states, where polarization refers to the orientation of the electric vector of an electromagnetic wave. Manipulating the combination of transmitted and received, horizontal- and vertical-polarized signals can provide a variety of information about the Earth's surface, because a given material's backscatter properties differ based upon polarization orientation. The ability to simultaneously collect in multiple polarization states thus allows enhanced discrimination of surficial features and land surface change processes, including landcover types (Ulaby and Elachi, 1990).

Overview of Regional Geology

The geology of the western Alaska Range records the accretion of the Peninsular-Alexander-Wrangellia (PAW) composite island arc superterrane to the existing continental margin during the Late Jurassic and Early Cretaceous (Pflaker and Berg, 1994). During accretion, sediments shed from the continent and PAW were deposited into a discontinuous string of sedimentary basins within the closing ocean (Pflaker and Berg, 1994; Ridgway and others, 2002). The Kahiltna terrane represents a western example of these basins, and where flysch sediment onlap onto both the continent and PAW (for example, Silberling and others, 1994). Detrital zircons suggest sedimentation in the basin, and by inference, final docking, occurred about 90 Ma. Cretaceous and recent tectonic plate motion models suggest significant westward translation of the sedimentary basins including the Kahiltna terrane and PAW since that time (Graham and others, 2013).

Multiple periods of magmatism have influenced the western Alaska Range and intruded the Kahiltna terrane since accretion (Moll-Stalcup, 1994; Moll-Stalcup and others, 1994; Hart and others, 2004). Gold metallogenesis is spatially linked to two periods in the Cretaceous (Graham and others, 2013). Porphyry copper-gold-molybdenum (Cu-Au-Mo) deposits, exemplified by the Pebble deposit, are associated with ~100 to 89 Ma in a continental arc (for example, Anderson and others, 2013; Lang and others, 2013). After a period of relative quiescence, gold metallogenesis occurred in association with initial (~76 Ma to 66 Ma) igneous rocks that were part of a broader ~76 to ~50 Ma magmatic event. Porphyry Au-Cu deposits are hosted in 76 Ma dioritic intrusions at and near the Whistler deposit (Graham and others, 2013; Hames, 2014), whereas slightly younger ca. 71–67 Ma plutons, exemplified by the Estelle pluton, host sheeted quartz-arsenopyrite vein sets (Graham and others, 2013; Taylor and others, 2014). Predominantly base metal prospects are associated with some Tertiary plutonic events (U.S. Geological Survey, 2008).

Geologic Application

SAR has been used for geologic applications and has been demonstrated to be useful in delineating both geologic units and structures (for example, Hanks and Guritz, 1997; Perski, 2005). SAR was effective in delineating carbonate versus clastic rocks in part of the Arctic National Wildlife Refuge, Brooks Range, Alaska, owing to contrasting surface roughness, including size and angularity of scree on talus slopes (Hanks and Guritz, 1997). Pal and others (2006) reported that processed SAR data was effective for mapping lineaments in the Singhbhum Shear Zone, India, that were not recognized using electro-optical imagery such as Landsat (Pal and others, 2006). Notably, many of the mineral deposits along the shear zone are hosted within these fault systems. Thus, ALOS PALSAR has the potential to identify different geologic units and faults in the current study area and when coupled with other remotely-sensed or ground-collected datasets could help select prospective areas for mineral deposits.

Methods

A total of 129 ALOS PALSAR fine beam dual polarization (horizontal-horizontal (HH) + horizontal-vertical (HV)) scenes were used to generate the image mosaic presented here. The individual scenes were collected in 2007, 2009, and 2010 with the majority being collected in 2010 (fig. 1). Scenes considered for incorporation were limited to those collected between June and September to minimize snow cover. Each scene covered approximately 70 km by 60 km in area. The fine-beam polarization data offered moderate spatial resolution (12.5 m) that can better differentiate land cover features than single polarization data (Ulaby and Elachi, 1990; Liu and others, 2010). The archival ALOS PALSAR data are available to U.S. citizens who can register to download from Vertex, the Alaska Satellite Facility's Data Portal at https://vertex.daac.asf.alaska.edu/ (Alaska Satellite Facility, 2015).

ALOS PALSAR images were in a data format that required significant pre-processing using specialized SAR software called MapReady so the data could be fully utilized for scientific studies (Alaska Satellite Facility Engineering Group, 2013). All PALSAR scenes were radiometrically calibrated to sigma nought ($\sigma°$), which is the measure of the ratio of the power of the pulse sent by the sensor to the ground and then received by the antenna—known as backscatter (Maitre, 2008; Alaska Satellite Facility Engineering Group, 2013). This calibration helps to reduce inter-scene spectral variability. Terrain correction was also applied using digital elevation model (DEM) information (Gesch and others, 2009) in order to reduce geometric and radiometric distortions in areas with high relief. The correction improved the positional geospatial accuracy of each scene, and normalized the pixel values of areas in steep terrain (Ulander, 1996; Alaska Satellite Facility Engineering Group, 2013).

The calibrated, terrain-corrected PALSAR scenes were then mosaicked using the image processing software ERDAS IMAGINE 2013 (Hexagon Geospatial, 2014). Further normalization processes were implemented to address differences in digital number (DN) values (backscatter response) between some scenes, phenomena that were attributed to temporal and season differences between return visits when PALSAR data was collected. PALSAR data with low spectral continuity to the image mosaic (identified through qualitative visual inspection) were normalized to the image mosaic using linear regression methods (Ferretti and others, 2001; Hadjimitsis and others, 2009). These regressions were applied in areas of overlap between the image to be normalized and the mosaic. Non-vegetated cover pixels were used as control pixels to carry out the regression for the images to be normalized. The spectral values for the control pixel samples (for example, bare rock surfaces) were used because they were consistent between scene dates. Image normalization was done on spectrally dissimilar PALSAR scenes where needed until a suitable mosaic was produced.

Results

The map presented here is a three-band image composite produced from the dual polarization image mosaic, where band 1 = HH polarization, band 2 = HV polarization, and band 3 = the ratio of the HH and HV polarizations (for example, HH/HV). The image displays polarization information which is sensitive to the microwave region of the electromagnetic spectrum (wavelengths near 23.6 cm). The ALOS PALSAR mosaic has not been classified into discrete categories. However, a qualitative comparison indicates the colors and color combinations in the map generally relate to coarse land cover categories in the USGS National Landcover Database (NLCD) 2001 classification (Homer and others, 2004). The color variations and assigned categories are presented in the map explanation. The categories in the explanation reflect differences in surface roughness, water content, and topography. Barren land (alluvial fan, glacial moraine, exposed rock) appears yellow in some areas and a mixture of pink and purple in others. Forest vegetation is chartreuse while shrub/scrubland areas are purple. Water appears black and dark blue. Areas with snow and ice are dark green, and deep purple to pink. Only a qualitative assessment was done of landcover type in comparison to the NLCD 2001. Therefore, it is up to the user to establish their own classification.

Preliminary mapping results indicate that certain rock types can be differentiated based on SAR backscatter responses. Specifically, there is a contrast in coloration of sedimentary rocks (relatively uniform pink and purple) and igneous rocks (variable mixing with yellows) in the Tyonek, Lime Hills, McGrath, and Talkeetna quadrangles.

Figure 2 illustrates the strong contrast of the yellow coloration of the Mount Estelle pluton (red hachure; Reed and Elliott, 1970) and other smaller ~70 Ma plutons to the northeast (white hachure), to purple and pink coloration of the Cretaceous sedimentary rocks they intrude. While many of the plutons and associated volcanics of various ages can also have yellow coloration, this is not always the case (blue hachure). In figure 2 the Tordrillo Mountains and plutons to the west display varied coloration, with deep purple and blue with very sparse yellow coloration on their eastern, snow- and glacier-covered side, with more magenta and sparse yellow on the relatively snow- and ice-poor western side (fig. 2). This relationship indicates that snow and ice can influence coloration and classification. Vegetative cover also influences the coloration and classification. Where known geology is covered by vegetation, the ALOS PALSAR data indicate only vegetation and the underlying bedrock is not differentiated.

Qualitatively, linear breaks in ALOS PALSAR data align with many mapped faults (Plafker and others, 1994; Wilson and others, 2009; Koehler and others, 2012, 2013; Wilson and others, 2012; Koehler, 2013), and may define additional lineaments or faults (fig. 2). For example, several north-northeast-trending linear features are observed cutting across multiple igneous and volcanic rock units in a single band (band 1), and are identified as lineaments in an area 23 kilometers south of the town of Skwentna and south of the Hayes River (fig. 2). Additional post-processing of data like that presented here, combined with other geologic data could be effective for identifying igneous rocks and faults. Since both igneous rocks and faults can be important for focusing ore-depositing fluids, such analyses could be useful for targeting areas prospective for base- and precious-metal mineral occurrences.

Summary

Synthetic Aperture Radar (SAR) data were used to compile a map consisting of 129 ALOS PALSAR scenes over the Kahiltna terrane of Alaska. The scenes were calibrated, terrain corrected, and normalized to produce a continuous radar image mosaic. This radar mosaic provides a cloud-free remotely sensed dataset that can be useful when characterizing land cover and geology. In at least parts of the region, sedimentary and many igneous rocks are characterized by distinct color patterns, which could help define their extents. Additional lineaments were also identified locally. These findings suggest that SAR data, coupled with additional post-processing could help improve refinement of the geologic evolution and metallogenesis in this region.

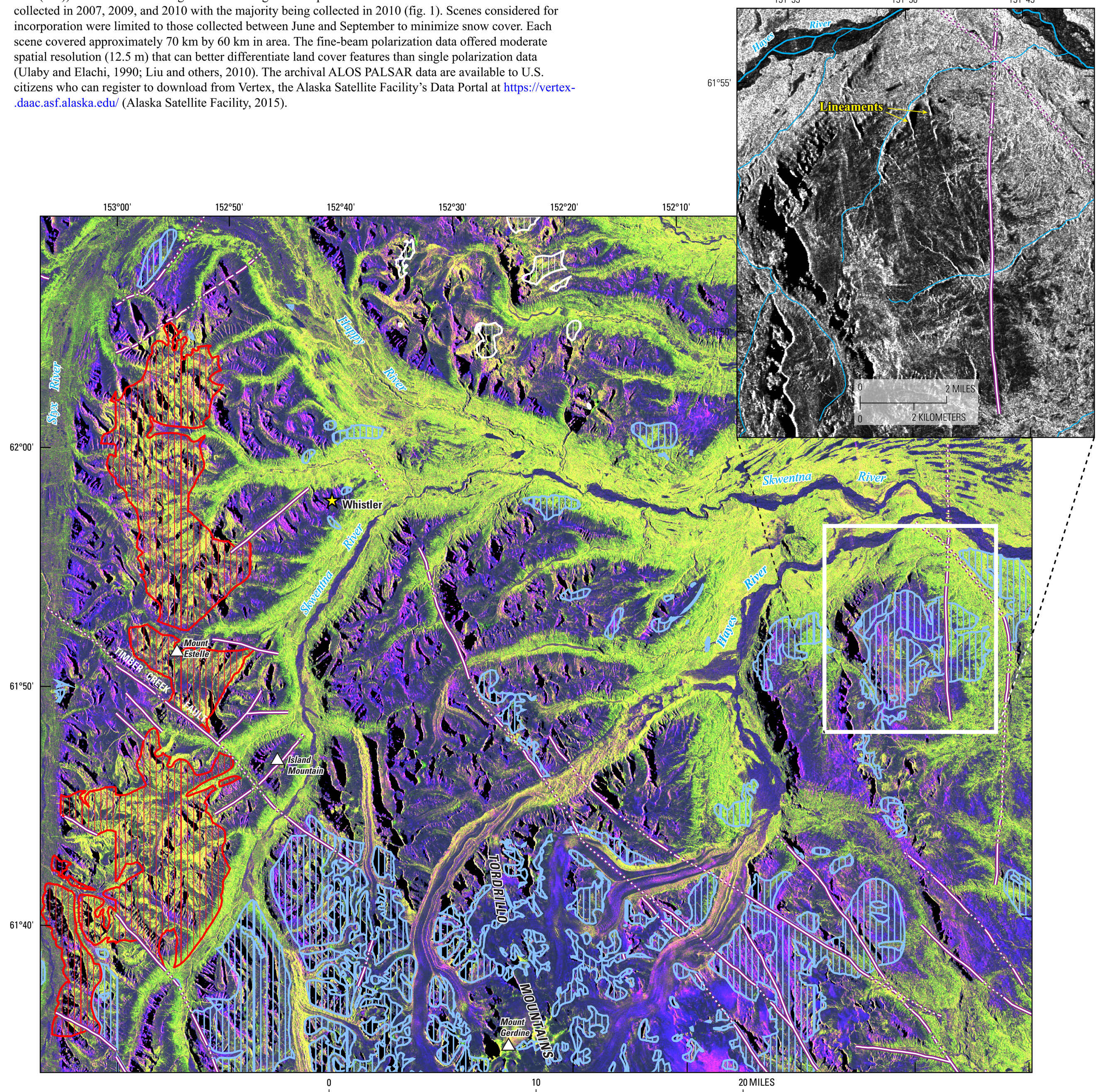

- **Fault**—Solid where accurately located, long dash where approximately located, short dash where inferred, and dotted where concealed
- **Mount Estelle pluton**—From Reed and Elliott, 1970; Wilson and others, 2009, 2012
- **70 Ma plutons**—From Wilson and others, 2009, 2012; Taylor and others, 2014
- **Plutonic rocks of other ages**—From Wilson and others, 2009, 2012; Taylor and others, 2014
- **Whistler deposit**

Figure 2. This 3-band image produced from the ALOS PALSAR mosaic shows the difference between geologic units of the Late Cretaceous intermediate to granitic plutonic rocks within the Estelle pluton (red hachures) and the surrounding Cretaceous sedimentary rocks (Reed and Elliott, 1970; Wilson and others, 2009, 2012). White and purple faults are from Wilson and others (2009, 2012). This area is a little more than 100 miles (161 km) northwest of Anchorage, Alaska. The smaller inset map shows a single band (band 1) ALOS PALSAR mosaic. Possible lineaments are indicated by yellow arrows; rivers in blue.

References Cited

Alaska Satellite Facility, 2015, Vertex—Alaska Satellite Facility Data Portal: Fairbanks, University of Alaska, Geophysical Institute, accessed January 9, 2015 at https://vertex.daac.asf.alaska.edu/.

Alaska Satellite Facility Engineering Group, 2013, ASF MapReady user manual version 3.1, 120 p. [Also available at https://media.asf.alaska.edu/uploads/pdf/mapready_manual_3.1.22.pdf.]

Anderson, E.D., Hitzman, M.W., Monecke, Thomas, Bedrosian, P.A., Shah, A.K., and Kelley, K.D., 2013, Geological analysis of aeromagnetic data from southwestern Alaska—Implications for exploration in the area of the Pebble porphyry Cu-Au-Mo deposit: Economic Geology, v. 108, p. 421–436.

Ferretti, Alessandro, Prati, Claudio, and Rocca, Fabio, 2001, Permanent scatterers in SAR interferometry: The Institute of Electrical and Electronics Engineers (IEEE) Transactions on Geoscience and Remote Sensing, v. 39, no.1, p. 8–20.

Gesch, D.B., Evans, G.A., Mauck, James, Hutchinson, John, and Carswell W.J., Jr., 2009, The National Map—Elevation: U.S. Geological Survey Fact Sheet 2009–3053, 4 p., accessed January 9, 2015, at http://pubs.usgs.gov/fs/2009/3053/.

Graham, G.E., Goldfarb, R.J., Gibler, M.L., and Roberts, M., 2013, Tectonic evolution and Cretaceous gold metallogenesis of southwestern Alaska, *in* Colpron, Maurice, Bissig, Thomas, Rusk, B.G., Thompson, J.F.H., eds., Tectonics, metallogeny, and discovery—The North American Cordillera and similar accretionary settings: Society of Economic Geologists, Special Publication, no. 17, p. 169–200.

Hadjimitsis, D.G., Clayton, C.R.I., and Retalis, Adrian, 2009, The use of selected pseudo-invariant targets for the application of atmospheric correction in multi-temporal studies using satellite remotely sensed imagery: International Journal of Applied Earth Observation and Geoinformation, v. 11, no. 3, p. 192–200.

Hames, B.P., 2014, Evolution of the Late Cretaceous Whistler Au-(Cu) porphyry corridor and magmatic-hydrothermal system, Kahiltna terrane, southwestern Alaska, USA: Vancouver, B.C., University of British Columbia, M.S. thesis, 415 p., accessed March 3, 2015, at https://elk.library.ubc.ca/handle/2429/50184/.

Hanks, C.L., and Guritz, R.M., 1997, Use of Synthetic Aperture Radar (SAR) for geologic reconnaissance in Arctic regions—An example from the Arctic National Wildlife Refuge, Alaska: American Association of Petroleum Geologists (AAPG) Bulletin, v. 81, no. 1, p. 121–134.

Hart, C.J., Mair, J.L., Goldfarb, R.J., and Groves, D.I., 2004, Source and redox controls on metallogenic variations in intrusion-related ore systems, Tombstone-Tungsten belt, Yukon Territory, Canada: Transactions of the Royal Society of Edinburgh, Earth Sciences, v. 95, p. 339–356.

Hexagon Geospatial, 2014, ERDAS IMAGINE—Complete Remote Sensing & Image Analysis: Norcross, Ga., Hexagon Geospatial, Intergraph Corp., accessed January 9, 2015, at http://www.hexagongeospatial.com/products/remote-sensing/erdas-imagine/.

Homer, Collin, Huang, Chengquan, Yang, Limin, Wylie, Bruce, and Coan, Michael, 2004, Development of a 2001 national land cover database for the United States: Photogrammetric Engineering and Remote Sensing, v. 70, no. 7, p. 829–840, accessed January 9, 2015, at http://www.mrlc.gov/pdf/July_PERS.pdf.

Japan Space Systems, 2012, PALSAR user's guide, (2d ed.): Tokyo, Japan Space Systems, 69 p. accessed on January 9. 2015, at http://gds.palsar.ersdac.jspacesystems.or.jp/e/guide/pdf/U_Guide_en.pdf/.

Koehler, R.D., 2013, Quaternary faults and folds (QFF): Alaska Division of Geological & Geophysical Surveys Digital Data Series 3, accessed on January 9, 2015, at http://maps.dggs.alaska.gov/qff/.

Koehler, R.D., Burns, P.A.C., and Weakland, J.R., 2013, Digitized faults of the neotectonic map of Alaska (Plafker and others, 1994), *in* Koehler, R.D., Quaternary Faults and Folds (QFF): Alaska Division of Geological & Geophysical Surveys, Miscellaneous Publication MP 150, accessed January 9, 2015, at http://www.dggs.alaska.gov/pubs/id/24791.

Koehler, R.D., Farrell, R.-E., Burns, P.A.C., and Combellick, R.A., 2012, Quaternary faults and folds of Alaska—A digital database: Alaska Division of Geological & Geophysical Surveys, Miscellaneous Publication 141, accessed January 9, 2015, at http://www.dggs.dnr.state.ak.us/pubs/id/23944.

Lang, J.R., Payne, J., Roberts, K., Reagliati, M., Oliver, J., and Roberts, K., 2013, Geology and magmatic-hydrothermal evolution of the giant Pebble porphyry copper-gold-molybdenum deposit, southwest Alaska: Economic Geology, v. 108, p. 437–462.

Liu, Xiuguo, Li, Yongsheng, Gao, Wei, and Xiao, Lin, 2010, Double polarization SAR image classification based on object-oriented technology: Journal of Geographic Information Systems, v. 2, p. 113–119.

Maitre, Henri, 2008, Processing of Synthetic Aperture Radar (SAR) Images: Hoboken, New Jersey, John Wiley and Sons, 382 p.

Moll-Stalcup, E.J., 1994, Latest Cretaceous and Cenozoic magmatism in mainland Alaska, *in* Plafker, George, and Berg, H.C., eds., The Geology of Alaska—The geology of North America: Geological Society of America, v. G–1, p. 589–618. [Available online at http://www.dggs.alaska.gov/pubs/id/22298.]

Moll-Stalcup, E.J., Brew, D.A., and Vallier, T.L., 1994, Latest Cretaceous and Cenozoic magmatic rocks of Alaska, *in* Plafker, George, and Berg, H.C., eds., The geology of Alaska—The geology of North America: Geological Society of America, v. G–1, 2 sheets, scale 1:2,500,000. [Available online at http://www.dggs.alaska.gov/pubs/id/22322.]

Pal, S.K., Majumdar, T.J., and Bhattacharya, A.K., 2006, Extraction of linear and anomalous features using ERS SAR data over Singhbhum shear zone, Jharkhand using fast Fourier transform: International Journal of Remote Sensing, v. 27, no. 20, p. 4513–4528.

Perski, Zbigniew, 2005, Application of SAR imagery and SAR interferometry in digital geological cartography, *in* Ostaficzuk, S.R., ed., The current role of geological mapping in geosciences, Proceedings of the NATO Advanced Research Workshop on Innovative Applications of GIS in Geological Cartography, Kazimierz Dolny, Poland 24–26 Nov. 2003, National Atlantic Treaty Organization (NATO) Science Series IV, Earth and environmental sciences: The Netherlands, Springer, v. 56, chap. 22, p. 225–244.

Plafker, George, and Berg, H.C., 1994, Overview of the geology and tectonic evolution of Alaska, *in* Plafker, George, and Berg, H.C., eds., The geology of Alaska—The geology of North America: Geological Society of America, v. G–1, p. 989–1021. [Available online at http://www.dggs.alaska.gov/pubs/id/22313.]

Plafker, George, Gilpin, L.M., and Lahr, J.C., 1994, Neotectonic map of Alaska, *in* Plafker, George, and Berg, H.C., eds., The geology of Alaska—The geology of North America: Geological Society of America, v. G–1, 2 sheets, scale 1:2,500,000. [Available online at http://dggs.alaska.gov/pubs/id/22331.]

Reed, B.L., and Elliott, R.L., 1970, Reconnaissance geologic map, analyses of bedrock and stream-sediment samples, and an aeromagnetic map of parts of the southern Alaska Range: U.S. Geological Survey Open-File Report 70–271, 145 p., 4 sheets, scale 1:125,000.

Ridgway, K.D., Trop, J.M., Nokleberg, W.J., Davidson, C.M., and Eastham, K.D., 2002, Mesozoic and Cenozoic tectonics of the eastern and central Alaska Range—Progressive basin development and deformation within a suture zone: Geological Society of America Bulletin, v.115, p. 1480–1504.

Silberling, N.J., Jones, D.L., Monger, J.W.H., Coney, P.J., Berg, H.C., and Plafker, George, 1994, Lithotectonic terrane map of Alaska and adjacent parts of Canada, *in* Plafker, George, and Berg, H.C., eds., The geology of Alaska—The geology of North America: Geological Society of America, v. G–1, 1 sheet, scale 1:2,500,000. [Available online at http://www.dggs.alaska.gov/pubs/id/22319.]

Taylor, R.D., Graham, G.E., Anderson, E.D., and Selby, David, 2014, Timing of ore-related magmatism in the western Alaska Range, southwestern Alaska: U.S. Geological Survey Open-File Report 2014–1115, 25 p., accessed March 3, 2015, at http://dx.doi.org/10.3133/ofr20141115/.

Ulaby, F.T., and Elachi, Charles, eds., 1990, Radar polarimetry for geoscience applications: Norwood, Mass., Artech House Publishers, 376 p.

Ulander, L.M.H., 1996, Radiometric slope correction of synthetic-aperture radar images: The Institute of Electrical and Electronics Engineers (IEEE) Transactions on Geoscience and Remote Sensing, v. 34, no. 5, p. 1115–1122.

U.S. Geological Survey, 2008, Alaska Resource Data File (ARDF), U.S. Geological Survey Open-File Report 2008–1225, accessed January 9, 2015, at http://mrdata.usgs.gov/ardf/.

Wilson, F.H., Hults, C.P., Schmoll, H.R., Haeussler, P.J., Schmidt, J.M., Yehle, L.A., and Labay, K.A., comps., digital files prepared by Wilson, F.H., Hults, C.P., Labay, K.A., and Shew, Nora, 2009, Preliminary geologic map of the Cook Inlet region, Alaska—Including parts of the Talkeetna, Talkeetna Mountains, Tyonek, Anchorage, Lake Clark, Kenai, Seward, Iliamna, Seldovia, Mount Katmai, and Afognak 1:250,000-scale quadrangles: U.S. Geological Survey Open-File Report 2009–1108, scale 1:250,000, accessed January 9, 2015, at http://pubs.usgs.gov/of/2009/1108/.

Wilson, F.H., Hults, C.P., Schmoll, H.R., Haeussler, P.J., Schmidt, J.M., Yehle, L.A., and Labay, K.A., comps., 2012, Geologic map of the Cook Inlet region, Alaska, including parts of the Talkeetna, Talkeetna Mountains, Tyonek, Anchorage, Lake Clark, Kenai, Seward, Iliamna, Seldovia, Mount Katmai, and Afognak 1:250,000-scale quadrangles: U.S. Geological Survey Scientific Investigations Map 3153, 76 p., 2 sheets, scale 1:250,000, accessed January 9, 2015, at http://pubs.usgs.gov/sim/3153/.

CONVERSION FACTORS

Multiply	By	To obtain
centimeter (cm)	0.3973	inch (in)
meter (m)	3.281	foot (ft)
kilometer (km)	0.6214	mile (mi)
square kilometer (km^2)	0.3861	square mile (mi^2)

Publishing support provided by:
Denver Publishing Service Center
Edit and digital layout by L.J. Binder
Manuscript approved for publication April 6, 2015

To learn about the USGS and its information products visit
http://www.usgs.gov/
1-888-ASK-USGS

This report is available at:
http://pubs.usgs.gov/sim/3323

ISSN 2329-132X (online)
http://dx.doi.org/10.3133/sim3323

For more information concerning this publication, contact:

Center Director, USGS Crustal Geophysics and Geochemistry Science Center
Box 25046, Mail Stop 964
Denver, Colo., 80225
(303)236-1312

Or visit the Crustal Geophysics and Geochemistry Science Center Web site at:
http://crustal.usgs.gov

Suggested citation: Cole, C.J., Johnson, M.R., and Graham, G.E., 2014, Advanced Land Observing Satellite (ALOS) Phased Array Type L-Band Synthetic Aperture Radar (PALSAR) mosaic for the Kahiltna terrane, Alaska, 2007–2010: U.S. Geological Survey Scientific Investigations Map, 1 sheet, scale 1:1,000,000, http://dx.doi.org/10.3133/sim3323.